



**HAL**  
open science

# Construction of Au quantum dots/nitrogen-defect-enriched graphite carbon nitride heterostructure via photo-deposition towards enhanced nitric oxide photooxidation

Yanzhi Liu, Lei Xu, Cheng Xie, Qianjun Ye, Zhaohui Han, Bochuan Zhang, Mickael Capron, Vitaly Ordonsky

## ► To cite this version:

Yanzhi Liu, Lei Xu, Cheng Xie, Qianjun Ye, Zhaohui Han, et al.. Construction of Au quantum dots/nitrogen-defect-enriched graphite carbon nitride heterostructure via photo-deposition towards enhanced nitric oxide photooxidation. *Journal of Colloid and Interface Science*, 2024, 670, pp.635-646. 10.1016/j.jcis.2024.05.103 . hal-04780060

**HAL Id: hal-04780060**

**<https://hal.science/hal-04780060v1>**

Submitted on 13 Nov 2024

**HAL** is a multi-disciplinary open access archive for the deposit and dissemination of scientific research documents, whether they are published or not. The documents may come from teaching and research institutions in France or abroad, or from public or private research centers.

L'archive ouverte pluridisciplinaire **HAL**, est destinée au dépôt et à la diffusion de documents scientifiques de niveau recherche, publiés ou non, émanant des établissements d'enseignement et de recherche français ou étrangers, des laboratoires publics ou privés.

# Photodeposition Au nanoparticles on g-C<sub>3</sub>N<sub>4</sub> toward enhancing oxidation of NO

Yanzhi Liu<sup>a, b, #</sup>, Lei Xu<sup>a, b, \*</sup>, Cheng Xie<sup>a, b, #</sup>, Qianjun Ye<sup>a, b</sup>, Zhaohui Han<sup>a, b</sup>,  
Bochuan Zhang<sup>a, b</sup>, Mickael Capron<sup>c, \*</sup> and Vitaly Ordonsky<sup>c, \*</sup>

<sup>a</sup> National Local Joint Laboratory of Engineering Application of Microwave Energy and Equipment Technology, Faculty of Metallurgical and Energy Engineering, Kunming University of Science and Technology, Kunming 650093, PR China

<sup>b</sup> The Key Laboratory of Unconventional Metallurgy, Ministry of Education, Kunming 650093, PR China

<sup>c</sup> Unité de Catalyse et Chimie du Solide, UMR CNRS 8181, Université de Lille, F-59000 Lille, France

\* Corresponding author: Tel: +86 0871 65138997; Fax: +86 0871 65138997

E-mail address: Lei Xu (xu\_lei@kust.edu.cn, xulei\_kmust@aliyun.com), Mickael Capron (mickael.capron@univ-lille.fr), Vitaly Ordonsky (vitaly.ordonsky@univ-lille.fr)

# These authors contributed equally to this work and should be considered co-first authors

## Abstract

The mitigation of pollution resulting from industrial waste gas emissions is a challenging academic and industrial problem. This study focused on the successful preparation of Au/g-C<sub>3</sub>N<sub>4</sub> composite material by photodeposition of Au nanoparticles onto the surface of g-C<sub>3</sub>N<sub>4</sub>. The composite catalyst exhibited robust photooxidation activity and stability in the oxidation of nitric oxide (NO) when subjected to visible light irradiation. As cocatalysts, Au nanoparticles *in-situ* grow on the surface of g-C<sub>3</sub>N<sub>4</sub>, forming a tight heterostructure with Schottky junction through van der Waals force, which enhances the SPR effect of Au nanoparticles, thereby enhancing the light absorption capacity of g-C<sub>3</sub>N<sub>4</sub> within the visible region, promoting the separation of electron-hole pairs generated during photooxidation, prolonging the lifetime of photogenerated carriers and enhancing the photooxidation capacity of the composites.

The mechanism of NO photooxidation has been proposed based on *in-situ* infrared spectroscopy and DFT calculations. This research serves as a valuable reference for the construction of semiconductor-cocatalyst systems and their behavior in NO photooxidation, contributing to the advancement of this field.

**Key words:** Carbon nitride; Au nanoparticles; Photodeposition; SPR; Photooxidation  
NO

## 1.Introduction

In recent years, as society and science have advanced, the release of industrial waste gas and water has caused serious pollution deteriorating our ecological environment [1]. As a common acid gas pollutant, NO poses numerous concerns including the generation of acid rain, depletion of the ozone layer, the formation of photochemical smog and haze, and the potential harm to human lung tissue [2-5]. Traditional methods such as the physical and chemical treatments, thermal catalytic reduction and biochemical method have obvious defects and limitations, such as high operational expenses, low efficiency, inadequate selectivity, incomplete degradation and transformation of pollutants, as well as a propensity to generate secondary pollutants [6]. Therefore, the exploration of environmentally friendly, efficient and non-secondary pollution degradation technologies has emerged as a focal point of research. Among these, semiconductor photocatalysis technology has garnered significant attention as a green, non-toxic, and sustainable degradation method.

As a typical 2D non-metallic polymer semiconductor photocatalyst, graphite-phase carbon nitride (g-C<sub>3</sub>N<sub>4</sub>) possesses several key advantages including its affordability, robust chemical stability, and straightforward synthesis process [7]. However, single component g-C<sub>3</sub>N<sub>4</sub> has non-ignorable disadvantages such as low utilization efficiency under visible light and easy recombination of photogenerated carriers, which limits its application in photocatalysis [8]. In order to overcome the defects of g-C<sub>3</sub>N<sub>4</sub>, researchers have proposed effective strategies [9-13] to improve its photocatalytic performances. For example, Zhang et al. [14] successfully incorporated WO<sub>x</sub> layers with oxygen vacancies into Au-modified g-C<sub>3</sub>N<sub>4</sub> nanosheets to form heterojunctions with excellent CO<sub>2</sub>

photoreduction properties. Wang et al. [15] effectively promoted the separation of photogenerated electrons and holes using composite of TiO<sub>2</sub> and g-C<sub>3</sub>N<sub>4</sub>. However, TiO<sub>2</sub> has poor optical absorption performance in the visible range. Noble metal nanoparticles have a surface plasmonic resonance effect (SPR), wherein the localized electric field they generate enhances the absorption of composite materials to visible light. Meanwhile, noble metal nanoparticles can be used as a trap to capture photoexcited electrons in semiconductors to improve the separation efficiency of photogenerated electron-hole pairs in semiconductor catalysts [16]. Therefore, loading noble metal can improve the photocatalytic performances of semiconductors. The Pt/g-C<sub>3</sub>N<sub>4</sub> composite prepared by Zhu et al. [17] through *in-situ* photoreduction improved the photocatalytic hydrogen evolution performances, compared with pure g-C<sub>3</sub>N<sub>4</sub>. The Ag/g-C<sub>3</sub>N<sub>4</sub>/TiO<sub>2</sub> and Ag/ZSM-5/g-C<sub>3</sub>N<sub>4</sub>/TiO<sub>2</sub> catalysts prepared by Wang et al. [18] can significantly improve the degradation efficiency of formaldehyde. Li et al. [19] synthesized Au/g-C<sub>3</sub>N<sub>4</sub> nanocomposites by *in-situ* wet chemical reduction method. The introduction of Au NPs improved the photocatalytic nitrogen oxide removal activity of g-C<sub>3</sub>N<sub>4</sub>. Faisal et al. [20] prepared an Au/g-C<sub>3</sub>N<sub>4</sub> composite photocatalyst, which showed high photocatalytic activity for the degradation of methylene blue dye and the drug Gemefloxacin mesylate within the range of visible light. Therefore, Au nanoparticles are considered a suitable cocatalyst to improve the photocatalytic efficiency of g-C<sub>3</sub>N<sub>4</sub>.

In this study, g-C<sub>3</sub>N<sub>4</sub>-Au composite photocatalyst was synthesized by photodeposition strategy. With NO as the target pollutant, the photocatalytic performances of the composite were studied. The material structure, elemental composition, morphology, optical properties and photooxidation activity of the best composite specific photocatalyst was analyzed by a series of characterization methods. Compared with pure g-C<sub>3</sub>N<sub>4</sub>, the photooxidation removal efficiency of g-C<sub>3</sub>N<sub>4</sub>-Au-3 under visible light can reach 77.4 % within 30 min. The test results show that the SPR effect of precious metals promotes the absorption of visible light by the sample, and it is easier to generate photogenerated charge carriers. AuNPs with a particle size of about 10 nm are *in-situ* grown on the surface of g-C<sub>3</sub>N<sub>4</sub>. Thus, the Au-g-C<sub>3</sub>N<sub>4</sub> heterojunction was constructed, and the tight interface enhanced the SPR

effect of Au and helped charge transport, promotes the separation of photogenerated electron-hole pairs, prolongs the lifetime of photogenerated carriers, and significantly improves the photooxidation activity. The mechanism of NO photooxidation was preliminarily revealed by *in-situ* infrared spectroscopy. DFT calculation shows that the introduction of Au nanoparticles can promote the photooxidation reaction.

## 2. Experimental section

### 2.1 Materials

Urea ( $\text{CH}_4\text{N}_2\text{O}$ , purity $\geq$ 99.0 %), chloroauric acid ( $\text{AuCl}_3\cdot\text{HCl}\cdot 4\text{H}_2\text{O}$ , purity $\geq$ 99.0 %), ethanol ( $\text{C}_2\text{H}_6\text{O}$ , purity $\geq$ 99.7 %) are supplied by the McLean's reagent. Also, secondary distilled water is utilized for all experiments. All gas purchase from Stone Head Gas Products LLC. The NO (10 ppm) bottle contains  $\text{N}_2$  equilibrium NO.

### 2.2 Photocatalyst preparation

Preparation process of g- $\text{C}_3\text{N}_4$ : 10 g urea was put into a ceramic crucible with a lid, which was heated in a box Muffle furnace at 550 °C for 2 h at a heating rate of 2.5 °C·min<sup>-1</sup>. The crucible was cooled to room temperature and then ground to obtain light-yellow powders of g- $\text{C}_3\text{N}_4$ .

Preparation process of g- $\text{C}_3\text{N}_4$ -Au: g- $\text{C}_3\text{N}_4$ -Au were prepared by photo-deposition method. In a typical process ,0.5 g prepared g- $\text{C}_3\text{N}_4$  were dispersed to 100 ml secondary distilled water by ultrasonic treatment for 30 min, a certain amount of chloroauric acid (0.025 mol·L<sup>-1</sup>) were added into the suspension drop by drop under magnetic stirring, and continue stirring for 60 min. At room temperature, the mixed solution was stirred under xenon lamp with 350 W and illuminated for 1.5 h, the product was centrifuged at 8000 rpm for 10 min and washed repeatedly with deionized water and ethanol, then dried in 333 K constant temperature oven for 24 h. The g- $\text{C}_3\text{N}_4$ -Au composites with mass fraction of Au about 1 %, 3 % and 5 % were named g- $\text{C}_3\text{N}_4$ -Au-1, g- $\text{C}_3\text{N}_4$ -Au-3 and g- $\text{C}_3\text{N}_4$ -Au-5, respectively.

### 2.3 Characterizations

Phase analysis was performed by X-ray diffractometer (D8, Bruker AXS GmbH, Germany). The Cu target is the radiation source ( $\lambda= 0.15418$  nm), the voltage is 40

kV, the current is 40 mA, and the  $2\theta$  range of X-ray diffraction detection is  $10^\circ$ - $80^\circ$ . Scanning electron microscopy (SEM, JSM 7401F, JEOL, Japan) and transmission electron microscopy (TEM, Tecnai G2 TF30, FEI, USA) were used to characterize the micromorphology of the composites. The elemental composition of the composites was analyzed by energy dispersive X-ray spectrometer (EDS) equipped with transmission electron microscope. The surface compositions, chemical valence states and valence band spectrum of the composites were analyzed by X-ray photoelectron spectroscopy (XPS, XSAM-800). The composites were diluted with potassium bromide powder, and the changes of functional groups of the photocatalysts were analyzed by Fourier Transform infrared spectrometer (FT-IR, Tensor27, Bruker) at the wave number of  $400$ - $4000\text{ cm}^{-1}$ . Photoluminescence (PL) spectra were measured using a fluorescence spectrometer (F-7000 FL, Hitachi, Japan) with an excitation wavelength of 325 nm. The UV-visible diffuse reflectance spectrum (DRS) of the photocatalyst was measured by UV-2550, Shimadzu, Japan. After the composites were degassed at  $200^\circ\text{C}$  for 6 h, the  $\text{N}_2$  adsorption-desorption isotherm was measured by adsorption analyzer (Mike ASAP2460). Electron spin resonance (ESR) spectra were obtained using A300 spectrometers ( Bruker, Germany) for the detection of free radical active species. The electrochemical characteristics of the composites were analyzed on CHI 604E electrochemical analyzer (CH Instruments Inc.). Platinum wire was used as the counter electrode, calomel reference electrode and working electrode. Using  $0.5\text{ mol/LNa}_2\text{SO}_4$  as electrolyte, the photoelectric response was tested by turning on and off the light source regularly.

## **2.4. Photocatalytic performance test**

### **2.4.1 Photooxidation NO Oxidation**

NO gas was oxidized in a quartz tube reactor at room temperature in order to evaluate the photocatalytic activity of the prepared composites. A 300 W xenon lamp was used to simulate a visible light source, in which the UV was cut off by a filter ( $\lambda > 420\text{ nm}$ ) placed vertically above the reactor. An on-line NO<sub>x</sub> detector (Model HNAG1000-4ST, Honeyeagle) was used to continuously record the concentration of NO at the reactor outlet. The specific experimental reaction system is shown in S1. The

0.025 g photocatalyst was weighed and placed in the quartz tube, the flow rate of compressed air and NO was controlled at 350 mL·min<sup>-1</sup> and 70 mL·min<sup>-1</sup>, respectively, by a mass flow controller. NO/Air flow passes through the reactor after complete premix through the humidification chamber. After the adsorption and desorption equilibrium is completed and the concentration of mixed gas was stable to 300 ppb, light is turned on for photooxidation reaction. The concentration of NO at the outlet of the reactor was continuously recorded by NO detector, and the removal ratio of NO oxidation was calculated as Eq. (1):

$$\eta (\%) = \frac{C_0 - C}{C_0} \times 100\% \quad (1)$$

Where  $\eta$  is the removal ratio of NO oxidation,  $C_0$  is the initial concentration of NO, ppb;  $C$  is the final concentration of NO, ppb.

#### 2.4.2 Capture experiment

The mechanism of photocatalysis was studied by the trapping experiment of active components. P-benzoquinone (BQ), disodium ethylenediamine tetraacetate (EDTA-2Na), and isopropanol (IPA) are used as inhibitors of  $\bullet\text{O}_2^-$ ,  $h^+$ , and  $\bullet\text{OH}$  produced in photooxidation reactions. Under the same conditions, the 0.025g photocatalyst was ultrasonically dispersed in 10 mL H<sub>2</sub>O with 0.001 mol of BQ, EDTA-2Na or IPA, respectively. It was dried at 60 ° C until the moisture was completely removed, and samples were collected for oxidative removal of 300 ppb of NO under visible light.

#### 2.4.3 *In-situ* infrared spectroscopy study of photoinduced NO oxidation process

The photooxidation pathway and reaction mechanism of NO under visible light were studied by *in-situ* Fourier transform infrared spectroscopy. The TENSOR II FT-IR spectrometer (Brüker) was tested alongside a high-temperature reaction chamber (HVC) and an *in-situ* diffuse reflection unit (Harrick). The 0.5 g sample was put into the reaction chamber and heat-treated at 110 °C for 1 h to drain the residual gas. The infrared diffuse reflection spectrum was used as the background, and the baseline was collected under dark conditions. Then the NO mixed gas was first passed through the humidification chamber and then into the reaction chamber (10 ppm NO cylinder, nitrogen as carrier gas, air mixing diluted NO concentration to 5 ppm). After adsorption

for 30 min, the visible light source 300 W xenon lamp ( $> 420$  nm filter) is open, and irradiates the photocatalyst, the infrared spectral data is record every 2 min, and scan in the range of  $4000\text{-}800\text{ cm}^{-1}$  [19].

#### 2.4.4 DFT Computational Details

All the density functional theory calculations were performed by using the Vienna ab initio Simulation Program (VASP) [21, 22]. The generalized gradient approximation (GGA) in the Perdew-Burke-Ernzerhof (PBE) form and a cutoff energy of 500 eV for planewave basis set were adopted [23]. A  $3 \times 3 \times 1$  Monkhorst-Pack grid was used for sampling the Brillouin zones at structure optimization [24]. The ion-electron interactions were described by the projector augmented wave (PAW) method [25]. The convergence criteria of structure optimization were chosen as the maximum force on each atom less than  $0.01\text{ eV}/\text{\AA}$  with an energy change less than  $1 \times 10^{-5}$  eV. The DFT-D3 semiempirical correction was described via Grimme's scheme method [26].

### 3. Results and discussion

The g-C<sub>3</sub>N<sub>4</sub>-Au photocatalyst was successfully prepared by photo-deposition method (Fig. 1(a)). From Fig. 1(b), g-C<sub>3</sub>N<sub>4</sub> shows an obvious sheet stacking structure with no obvious change after the introduction of Au (Fig. 1(c)). Further observations of the composites by transmission electron microscopy (TEM) show that Au nanoparticles with a size of about 10 nm are well distributed on the surface of g-C<sub>3</sub>N<sub>4</sub> (Fig. 1(d)). The high-resolution transmission electron microscopy (HR-TEM) image (Fig 1(e)) reveals a lattice spacing of 0.235 nm, which corresponds to the crystal plane of face-centered cubic Au (1 1 1) [27]. The element mapping (Fig. 1(f)) shows the uniform distribution of C, N and Au in the catalyst [28].

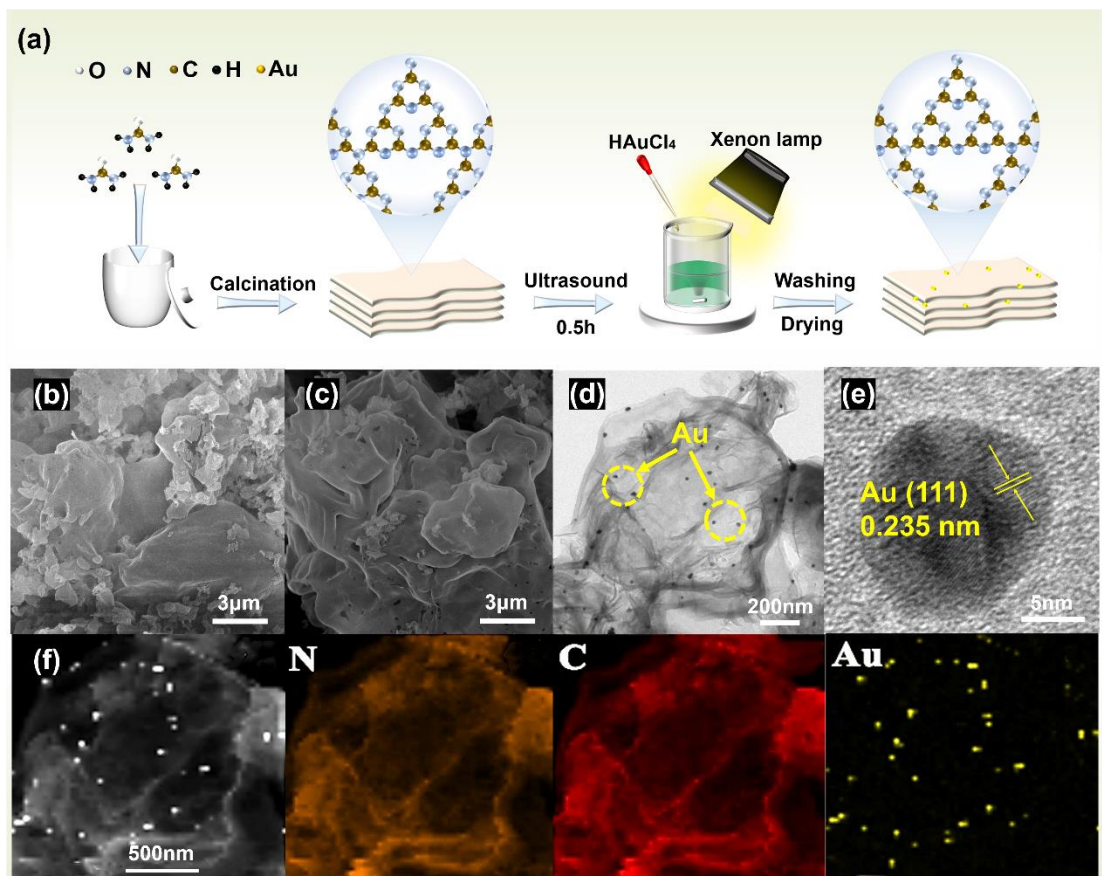


**Fig. 1** Preparation process and microstructure of samples: (a) synthesis of g-C<sub>3</sub>N<sub>4</sub> and g-C<sub>3</sub>N<sub>4</sub>-Au, (b, c) SEM patterns of g-C<sub>3</sub>N<sub>4</sub> and g-C<sub>3</sub>N<sub>4</sub>-Au nanocomposites, (d) TEM image of g-C<sub>3</sub>N<sub>4</sub>-Au-3 nanocomposites, (e) HR-TEM image, (f) the elemental mapping images

As shown in Fig. 2(a), all materials show characteristic diffraction peaks at 13.3° and 27.4° of (1 0 0) and (0 0 2) lattice planes of g-C<sub>3</sub>N<sub>4</sub>, respectively, reflecting the in-plane structure stacking motif and the interlayer structure stacking [29]. As the loading percentage of Au nanoparticles (AuNPs) on g-C<sub>3</sub>N<sub>4</sub> increases to 5 %, the X-ray diffraction (XRD) pattern exhibits distinct peaks at 38.23°, 44.24°, and 64.73° corresponding to the crystallographic planes of (1 1 1), (2 0 0), and (2 2 0) of the Au nanoparticles, respectively [30]. The chemical state of the composite surface was studied by X-ray photoelectron spectroscopy (XPS). Fig 2b shows the characteristic peaks at 284.8 eV, 286.4 eV and 288.2 eV in the C 1s high-resolution map of the composite, which are attributed to the C-C, C-O-H and N-C=N in g-C<sub>3</sub>N<sub>4</sub>, respectively [14]. The N 1s spectrum contains peaks at 398.8 eV and 400.5 eV corresponding to sp<sup>2</sup> hybrid

nitrogen (CN=C) and  $sp^3$  bonded nitrogen N-(C)<sub>3</sub>, respectively. Fig. 2(d) displays that the Au 4f high-resolution map of the composite material has two symmetric peaks near 84.2 eV and 87.8 eV, corresponding to Au 4f<sub>7/2</sub> and Au 4f<sub>5/2</sub>, which is consistent with the standard binding energy of zero-valence Au [31]. This indicates that Au nanoparticles are successfully loaded on g-C<sub>3</sub>N<sub>4</sub> matrix [32]. FTIR was used to study the surface functional groups and structural changes of the composites. The FTIR spectra of pure g-C<sub>3</sub>N<sub>4</sub> and g-C<sub>3</sub>N<sub>4</sub>-Au composites are shown in Fig. 2(e). The peak of all composites at 810 cm<sup>-1</sup> corresponds to the respiratory vibration of the tri-s-triazine ring in g-C<sub>3</sub>N<sub>4</sub>. Peaks in the 1200-1650 cm<sup>-1</sup> range (located at 1238, 1317, 1404, 1572 and 1637 cm<sup>-1</sup>) are caused by vibrations of aromatic C-N heterocyclic rings. The peaks of the sample in the range of 3100~3600 cm<sup>-1</sup> are attributed to the signals of O-H or N-H vibrations [33, 34].

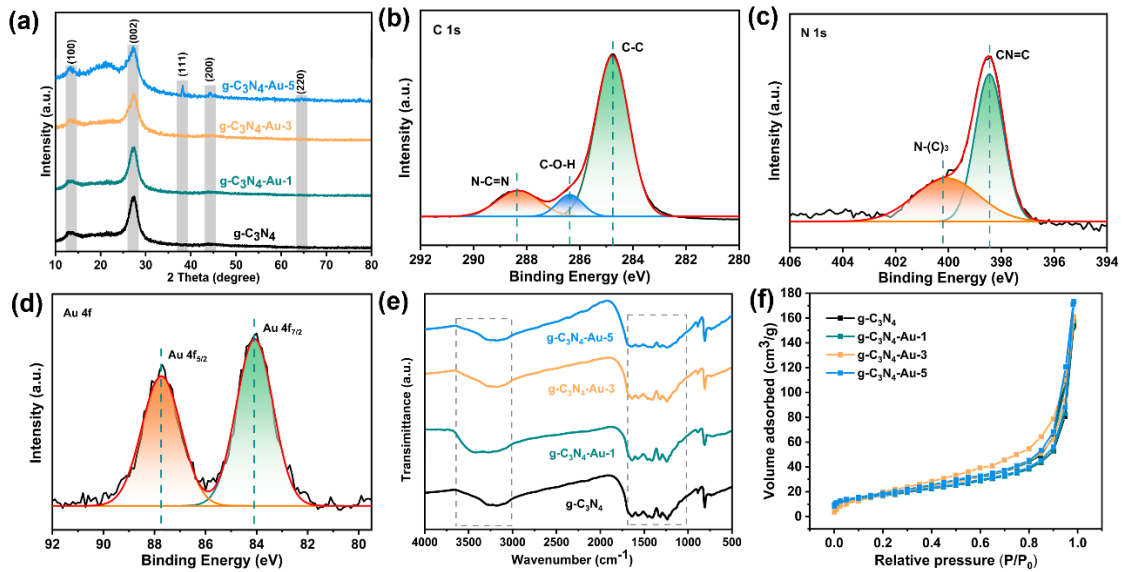


**Fig. 2** Phase structure and chemical composition of samples: (a) XRD spectra of g-C<sub>3</sub>N<sub>4</sub> and g-C<sub>3</sub>N<sub>4</sub>-Au nanocomposites, XPS spectra of g-C<sub>3</sub>N<sub>4</sub>-Au-3 nanocomposites: (b) C 1s, (c) N 1s, (d) Au 4f, (e) FT-IR spectra of g-C<sub>3</sub>N<sub>4</sub> and g-C<sub>3</sub>N<sub>4</sub>-Au nanocomposites, (f) the N<sub>2</sub> adsorption–desorption isotherms

The N<sub>2</sub> adsorption-desorption isotherms and the pore size distribution curve depicted in Fig. 2(f) were utilized for assessing the pore structure of the composites. By employing the Brunauer-Deming-Deming-Teller (BDDT) classification, it was determined that both pure g-C<sub>3</sub>N<sub>4</sub> and g-C<sub>3</sub>N<sub>4</sub>-Au composites exhibited IV-type curves

and displayed H3 hysteresis rings. These characteristics indicate the presence of mesoporous pores in the composites, which are formed between sheets of g-C<sub>3</sub>N<sub>4</sub>.<sup>[35, 36]</sup> This is consistent with the g-C<sub>3</sub>N<sub>4</sub> morphology observed by SEM in Fig. 1(a).

To assess the photooxidation properties of the composites under visible light, g-C<sub>3</sub>N<sub>4</sub>, g-C<sub>3</sub>N<sub>4</sub>-Au-1, g-C<sub>3</sub>N<sub>4</sub>-Au-3 and g-C<sub>3</sub>N<sub>4</sub>-Au-5 were used for oxidation of NO gas at a concentration of 300 ppb. Under visible light irradiation, the photocatalytic conversion rate of NO decreases rapidly within the first 5 min to stable catalytic activity. As shown in Fig. 3(a), g-C<sub>3</sub>N<sub>4</sub> modified with Au NPs enhanced the NO oxidation activity. The highest conversion rate of NO is observed over g-C<sub>3</sub>N<sub>4</sub>-Au-3 at 77.4 %, while the conversion rate of a pure g-C<sub>3</sub>N<sub>4</sub> under the same conditions is only 33.2 %, When the content of Au reached 5 %, the conversion ratio of NO decreased to 54.4 %, which indicated that a proper amount of AuNPs doping could improve the photocatalytic activity of g-C<sub>3</sub>N<sub>4</sub> for NO removal, this may be due to photodeposition forming tight Au-g-C<sub>3</sub>N<sub>4</sub> heterostructures on the g-C<sub>3</sub>N<sub>4</sub> surface, enhances the charge transfer, improves the separation efficiency of electron-hole pairs, and prolongs the life of photogenerated carriers, which is conducive to improve the photocatalytic activity<sup>[37]</sup>.

The catalytic results can be fitted by (Fig. 3(b)) the first-order kinetic model<sup>[38]</sup> (Eq.2)

$$\ln(C/C_0) = kt \quad (2),$$

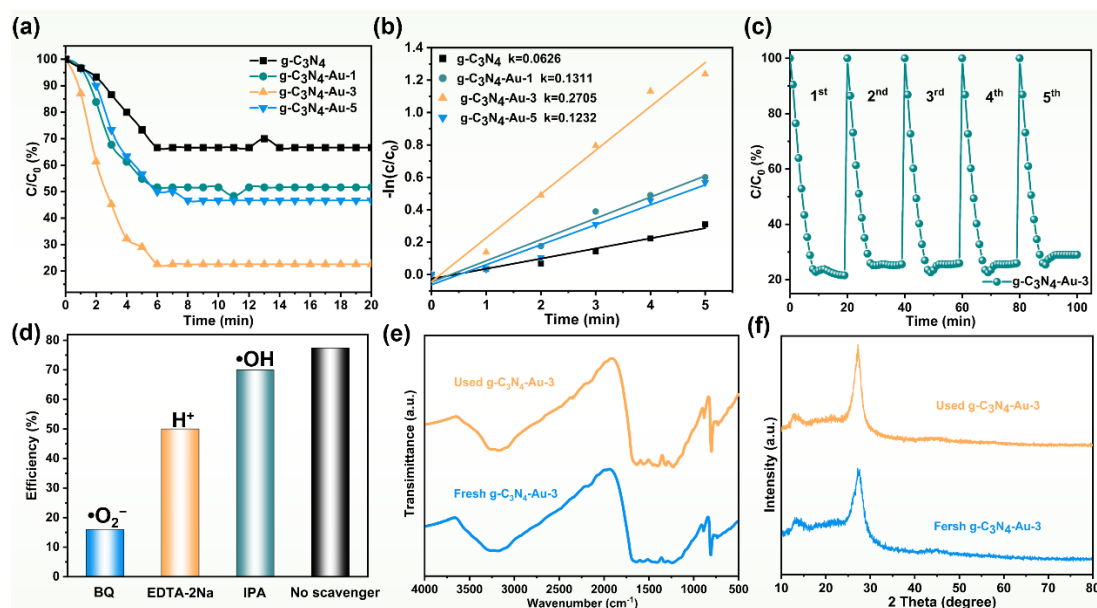
The kinetic constants decrease in the row g-C<sub>3</sub>N<sub>4</sub>-Au-3 (0.02705 min<sup>-1</sup>)> g-C<sub>3</sub>N<sub>4</sub>-Au-1 (k = 0.1232 min<sup>-1</sup>) ≈ g-C<sub>3</sub>N<sub>4</sub>-Au-5 (k = 0.1311 min<sup>-1</sup>)> g-C<sub>3</sub>N<sub>4</sub>. The kinetic results further indicate that the introduction of Au nanoparticles plays a key role in enhancing the performance of photooxidation capacity.

The catalyst stability is an important factor for practical applications. To test this, we reused g-C<sub>3</sub>N<sub>4</sub>-Au-3 and exposed it to visible light for five cycles. Fig. 3(c) shows that while the activity of g-C<sub>3</sub>N<sub>4</sub>-Au-3 decreased slightly, it remained mostly unchanged. This suggests that it has good photostability and can be used again.

In order to explore the photooxidation removal mechanism of NO by g-C<sub>3</sub>N<sub>4</sub>-Au, trapping experiments were conducted to determine the formation of active free radicals

involved in the oxidation removal of NO. P-benzoquinone (BQ), disodium ethylenediamine tetraacetate (EDTA-2Na), and isopropyl alcohol (IPA) were used as scavengers of  $\bullet\text{O}_2^-$ ,  $\text{h}^+$ , and  $\bullet\text{OH}$  produced in photocatalytic reactions. As can be seen from Fig. 3(d), the photooxidation efficiency of g-C<sub>3</sub>N<sub>4</sub>-Au-3 composite decreases from 77.4 % to 6 %, 50 % and 70 %, respectively, after the addition of BQ, EDTA-2Na and IPA. The results show that  $\bullet\text{O}_2^-$  is the main active radical in the photooxidative degradation of NO.  $\bullet\text{O}_2^-$  can be obtained by photogenerative electron reduction of O<sub>2</sub> adsorbed on the surface of the composite. Meanwhile,  $\text{h}^+$  at the VB of g-C<sub>3</sub>N<sub>4</sub>-Au cannot oxidize H<sub>2</sub>O to  $\bullet\text{OH}$  due to potential differences. Therefore, we speculate that  $\text{h}^+$  generated by photocatalysis can directly oxidize NO and enhance the photooxidation performance to a certain extent [39].

We analyzed the FTIR patterns and XRD patterns of the materials before and after recycling. Fig. 3(e, f) illustrates that the surface functional groups and crystal structure of the catalysts remained largely unchanged after cycling. Additionally, Table 1 provides a comparison of the NO removal performance of g-C<sub>3</sub>N<sub>4</sub>-Au-3 with other photocatalysts reported in previous studies. Li et al. [19] successfully loaded Au nanoparticles on g-C<sub>3</sub>N<sub>4</sub>-Au by reducing chloroauric acid with sodium borohydride, and the degradation rate reached 41% by using NO gas flow of 500 ppb. In this work, g-C<sub>3</sub>N<sub>4</sub> was excited under visible light to generate reducing electrons to effectively reduce chloroauric acid, and the deposited Au NPs had good dispersion and stability, which made the formation of a tight heterostructure between AuNPs and g-C<sub>3</sub>N<sub>4</sub>, which can improve the photooxidation activity of NO.



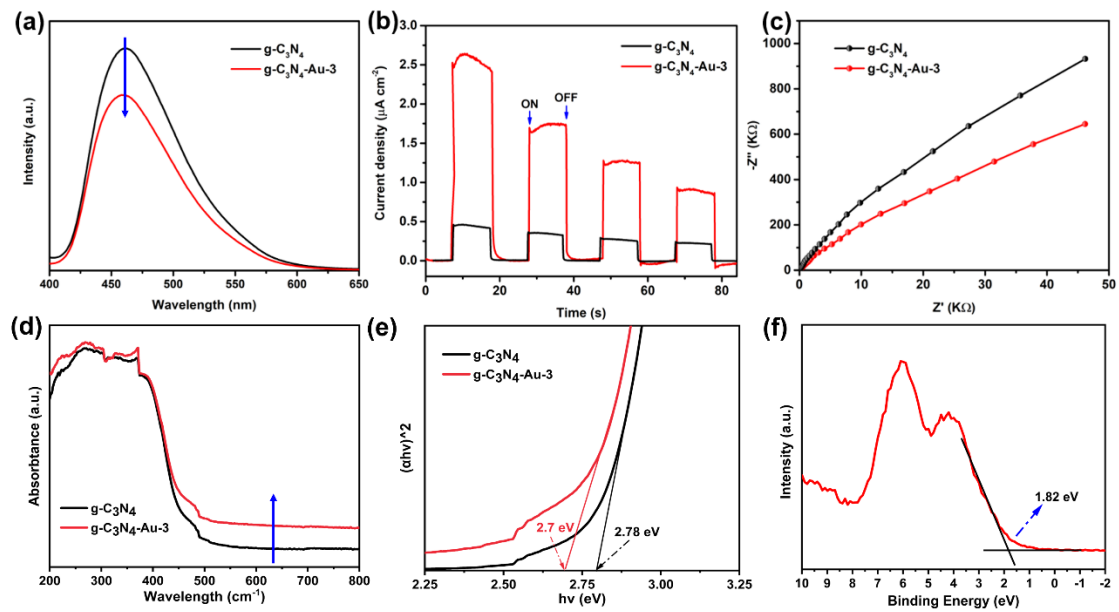
**Fig. 3** Performance and stability analysis of samples: (a) time-dependent oxidation removal of NO, (b) first-order kinetic curves of NO oxidation removal, (c) catalytic stability test for the g-C<sub>3</sub>N<sub>4</sub>-Au-3 photocatalyst, (d) effect of the trapping reagent on the oxidation removal of NO, (e) FTIR spectra and (f) XRD spectra of fresh and used g-C<sub>3</sub>N<sub>4</sub>-Au-3 composite

Table 1 NO removal performance of g-C<sub>3</sub>N<sub>4</sub>-Au-3 compared with other photocatalysts reported in the reference.

Photocatalyst	Initial concentration of NO	Oxidation removal ratio	light source	references
Pd/g-C <sub>3</sub> N <sub>4</sub>	2.2 ppm	56.30%	A 300W Xe lamp	[40]
S-doped g-C <sub>3</sub> N <sub>4</sub>	600 ppm	53%	A 150 W visible light LED lamp with filter ( $\lambda > 400$ nm)	[13]
Au/g-C <sub>3</sub> N <sub>4</sub>	500 ppb	41%	A 150 W commercial halogen tungsten lamp with filter ( $\lambda > 420$ nm)	[19]
Pd/g-C <sub>3</sub> N <sub>4</sub>	12 ppm	83%	A 300 W xenon lamp with filter ( $\lambda > 380$ nm)	[41]
WO <sub>x</sub> /Au/g-C <sub>3</sub> N <sub>4</sub>	600 ppb	61%	A 500 W Xe lamp	[14]
Ag/Bi <sub>2</sub> S <sub>3</sub>	500 ppb	31.12%	A 300 W solar lamp with filter ( $\lambda > 300$ nm)	[4]
Ag <sub>3</sub> PO <sub>4</sub> /g-C <sub>3</sub> N <sub>4</sub>	2 ppm	41.76%	A mercury lamp with filter (>290 nm)	[42]
black P/g-C <sub>3</sub> N <sub>4</sub>	600 ppb	74%	Two 300 W Xe lamps with filter ( $\lambda > 420$ nm)	[43]
Graphene quantum dots/g-C <sub>3</sub> N <sub>4</sub>	20 ppm	87%	A 300 W Xe lamp with filter ( $\lambda > 380$ nm)	[44]
Au/ZnIn <sub>2</sub> S <sub>4</sub> /g-C <sub>3</sub> N <sub>4</sub>	600 ppb	59.70%	A 300 W Xe lamp	[45]
TiO <sub>2</sub> /C/g-C <sub>3</sub> N <sub>4</sub>	100 ppm	94%	A 500 W Xe lamp with filter ( $\lambda > 420$ nm)	[46]
NiCoP/g-C <sub>3</sub> N <sub>4</sub>	600 ppb	78%	A 500 W Xe lamp	[47]
AgVO <sub>3</sub> /g-C <sub>3</sub> N <sub>4</sub>	600 ppb	65%	A 300 W Xe lamp	[48]
Au/g-C <sub>3</sub> N <sub>4</sub>	300 ppb	77.4%	A 300 W Xe lamp ( $\lambda > 420$ nm)	This work

PL spectra were used to characterize the separation and recombination of electron-hole pairs in composites [49]. The fluorescence intensity serves as an indicator of the separation rate of photogenerated carriers, with higher intensity indicating lower separation. In Fig. 4(a), it is observed that the fluorescence emission peak intensity of g-C<sub>3</sub>N<sub>4</sub>-Au-3 composites is significantly weaker compared to pure g-C<sub>3</sub>N<sub>4</sub>. This suggests that the introduction of Au effectively inhibits the recombination of photogenerated electron-hole pairs, thereby extending the lifespan of the photogenerated carriers. Furthermore, the photocurrent response and electron migration rate were analyzed using photocurrent and electrochemical impedance spectroscopy (EIS). In Fig. 4(b), it can be observed that the photocurrent response intensity of the composite is notably greater compared to pure g-C<sub>3</sub>N<sub>4</sub>. This indicates that the migration rate of photogenerated carriers in this sample is higher, which is advantageous for facilitating efficient photocatalytic reactions [50]. Furthermore, as depicted in Fig. 4(c), a smaller radius of curvature observed in the electrochemical impedance spectroscopy (EIS) indicates a lower impedance for the composite material [51]. This reduced impedance is favorable for the transmission of photogenerated carriers, aligning with the results obtained from the photocurrent tests. The photochemical characterization results demonstrate that the introduction of Au nanoparticles effectively enhances the separation of photogenerated electron-hole pairs, prolongs the lifetime of photogenerated carriers, reduces the resistance for carrier migration, and improves the photocatalytic performance. The optical properties of the samples were assessed using UV-vis measurements. Fig. 4(d) illustrates that the composite material exhibits significantly enhanced light absorption capacity within the visible light wavelength range compared to pure g-C<sub>3</sub>N<sub>4</sub>. This enhancement suggests that the surface plasmon resonance (SPR) effect of the noble metal (Au) improves the sample's response to visible light and enhances its photocatalytic performance [46]. In Fig. 4(e), the tauc diagram represents the band gap width spectrum of g-C<sub>3</sub>N<sub>4</sub> and g-C<sub>3</sub>N<sub>4</sub>-Au-3, calculated using the Kubelka-Munk formula. The tangents intersecting the X-axis indicate band gap widths of 2.7 eV and 2.78 eV for the g-C<sub>3</sub>N<sub>4</sub>-Au-3 and g-C<sub>3</sub>N<sub>4</sub>, respectively. Narrowing the band gap width allows for a broader range of light response,

thereby generating more excited electrons, which is beneficial for enhancing photocatalytic activity [52]. Apart from the number of surface holes and electrons, the photocatalytic activity of a photocatalyst is also influenced by the redox potential of surface holes and electrons. Therefore, the XPS valence band spectrum was measured to analyze the valence band potential of g-C<sub>3</sub>N<sub>4</sub>-Au-3. As shown in Fig. 4(g), the valence band potential of g-C<sub>3</sub>N<sub>4</sub>-Au-3 is 1.82 eV, and its band gap is 2.7 eV, as depicted in the tauc diagram. The conduction band potential (Ec) can be calculated using the formula  $E_g = E_v - E_c$ .

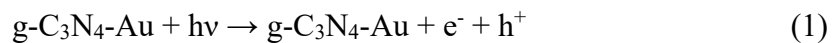


**Fig. 4** Analysis of charge separation, charge transfer and light adsorption: (a) the photoluminescence spectra, (b) the transient photocurrent response and (c) electrochemical resistance spectra of g-C<sub>3</sub>N<sub>4</sub> and g-C<sub>3</sub>N<sub>4</sub>-Au -3 nanocomposites, (d) UV-vis absorbance spectra, (e)  $E_g$  of g-C<sub>3</sub>N<sub>4</sub> and g-C<sub>3</sub>N<sub>4</sub>-Au -3 nanocomposites and (f) the XPS valence band spectrum

EPR was utilized to detect the reactive species produced during the photooxidation reaction under irradiation of visible light. 5, 5-dimethyl-1-pyrrolin-n-oxide (DMPO) acts as a trapping agent to trap  $\bullet\text{O}_2^-$  and  $\bullet\text{OH}$  [53]. It can be seen from Fig. 5(a, b), the composites exhibit obvious  $\bullet\text{OH}$  and  $\bullet\text{O}_2^-$  characteristic signals under visible light irradiation. Compared with pure g-C<sub>3</sub>N<sub>4</sub>, g-C<sub>3</sub>N<sub>4</sub>-Au-3 has a higher signal intensity, which indicates that g-C<sub>3</sub>N<sub>4</sub>-Au-3 can produce more  $\bullet\text{O}_2^-$  and

•OH to participate in the photocatalytic reaction. This is consistent with the results of PL and photochemical characterizations. The introduction of Au NPs promote the separation of photogenerated electron-hole pairs, extends the life of the carrier, and shows better photooxidation activity. Combined with the experimental results of free radical capture (Fig. 5(d)), as the signal of •OH detected by EPR, it can be inferred that •O<sub>2</sub><sup>-</sup>, as the main active free radical in the photocatalytic reaction process, can oxidize H<sub>2</sub>O to obtain •OH, thus enhancing the photooxidation activity.

The photo-oxidation of NO using g-C<sub>3</sub>N<sub>4</sub> and g-C<sub>3</sub>N<sub>4</sub>-Au-3 photocatalysts under visible light, as well as the reaction mechanism, were further investigated through *in-situ* Fourier transform infrared spectroscopy. In Fig. 5(c), the bands at 951 cm<sup>-1</sup> and 2970 cm<sup>-1</sup> correspond to nitrogen dioxide (NO<sub>2</sub>) after illumination. The peak position of 907 cm<sup>-1</sup> corresponds to N<sub>2</sub>O<sub>4</sub>, NO<sub>2</sub><sup>-</sup> is represented at 1106 cm<sup>-1</sup>, and (NO<sub>3</sub><sup>-</sup>) are observed at 1000 cm<sup>-1</sup> and 1048 cm<sup>-1</sup>. During this time, NO is primarily adsorbed on the catalyst's surface, and oxidation results in the formation of NO<sub>2</sub>. Pure g-C<sub>3</sub>N<sub>4</sub> exhibits high photogenerated electron-hole pair recombination efficiency, low visible light absorption capacity, and fewer active free radicals, leading to a single product and poor photocatalytic activity. Upon the introduction of Au nanoparticles, a new characteristic peak appears in the *in-situ* infrared spectrum of g-C<sub>3</sub>N<sub>4</sub>-Au-3, as shown in Fig. 5(d). This includes N<sub>2</sub>O<sub>4</sub> (907 cm<sup>-1</sup>), NO<sub>2</sub> (1067 cm<sup>-1</sup>), NO<sub>2</sub><sup>-</sup> (1125 cm<sup>-1</sup>), and NO<sub>3</sub><sup>-</sup> (1031 cm<sup>-1</sup>, 1048 cm<sup>-1</sup>, 1148 cm<sup>-1</sup>). Notably, compared to Fig. 5(c), the addition of AuNPs increases the peak intensity attributed to nitrate ions at 1048 cm<sup>-1</sup>, and new characteristic peaks of nitric acid at 1031 cm<sup>-1</sup> and 1148 cm<sup>-1</sup> emerge. Furthermore, the strong peak of NO<sub>2</sub> at 951 cm<sup>-1</sup> disappears in Fig. 5(d). It is speculated that the presence of AuNPs facilitates the oxidation and conversion of NO<sub>2</sub> to nitrate. The formation of new intermediates contributes to a more complex photocatalytic reaction process. Equation (1-9) is a proposed representation of the photooxidation removal pathway of NO:





According to the above-mentioned experiment results, the photocatalytic mechanism is proposed in Fig. 5(e). Under the irradiation of visible light, g-C<sub>3</sub>N<sub>4</sub> generates photogenerated electron-hole pairs, which are concentrated in the conduction band and valence band of g-C<sub>3</sub>N<sub>4</sub>. Au nanoparticles are anchored on the carbon nitride surface *in-situ* by photodeposition, and the contact surface form a heterojunction with Schottky junction due to the difference in the Fermi level, and excited electrons at the conduction band of g-C<sub>3</sub>N<sub>4</sub> are easily transferred to Au nanoparticles, which act as a trap for photogenerated electrons to promote electron transfer and improve the photogenerated carrier separation efficiency of semiconductor catalysts [54]. More importantly, as a cocatalyst, Au nanoparticles directly in contact with g-C<sub>3</sub>N<sub>4</sub> experience SPR under certain wavelength of light excitation, generate "hot electrons" that can cross the Schottky junction, and are injected into the conduction band of g-C<sub>3</sub>N<sub>4</sub> to participate in the photocatalytic reaction, as a result, the band gap energy decreases from 2.78 eV to 2.7 eV, which promotes the absorption of visible light by the composite, thus the photocatalytic efficiency of the photocatalyst is improved. Electrons can reduce the surface chemisorbed O<sub>2</sub> to  $\cdot\text{O}_2^-$ , and then react with H<sub>2</sub>O to generate  $\cdot\text{OH}$ . Due to potential differences,  $\cdot\text{OH}$  cannot be generated at the valence band of g-C<sub>3</sub>N<sub>4</sub> [55]. Therefore, the main active free radicals in this reaction is  $\cdot\text{O}_2^-$ , which NO can be oxidized to NO<sub>2</sub>, NO<sub>2</sub><sup>-</sup> and NO<sub>3</sub><sup>-</sup> and accumulate on the surface of the composites [42, 48].

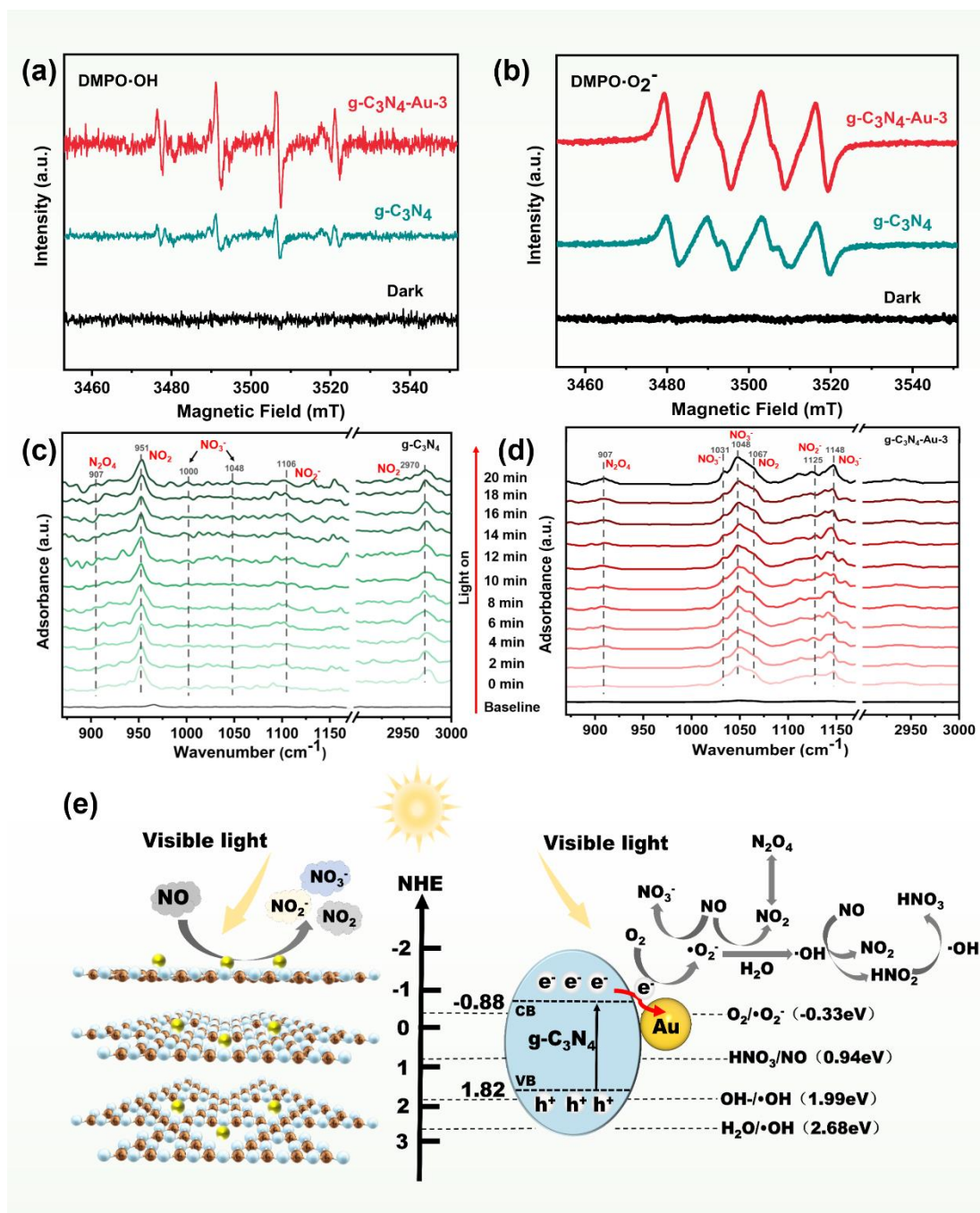


**Fig 5.** Radicals monitoring and simulation and photocatalysis reaction process: EPR spectra of (a) DMPO•OH and (b) DMPO•O<sub>2</sub><sup>-</sup> over the g-C<sub>3</sub>N<sub>4</sub> and g-C<sub>3</sub>N<sub>4</sub>-Au -3 nanocomposites, *in-situ* DRIFTS spectra of NO removal by photooxidation of (c) g-C<sub>3</sub>N<sub>4</sub> and (d) g-C<sub>3</sub>N<sub>4</sub>-Au (e) photocatalytic mechanism diagram of g-C<sub>3</sub>N<sub>4</sub>-Au composite

**Table 3** Assignments of the IR bands during photooxidation of NO process during visible-light irradiation

Wavenumbers (cm <sup>-1</sup> )	Assignment	References
907	N <sub>2</sub> O <sub>4</sub>	[3]
951	NO <sub>2</sub>	[56]
1000	bridging nitrates	[57]
1031	NO <sub>3</sub> <sup>-</sup>	[56]
1048	NO <sub>3</sub> <sup>-</sup>	[58]
1067	NO <sub>2</sub>	[39]
1106	bi/monodentate nitrites	[56]
1125	NO <sub>2</sub> <sup>-</sup>	[39]
1148	monodentate nitrates	[57]
2970	NO <sub>2</sub>	[59]

In order to explore the effect of the introduction of AuNPs on the adsorption activation of NO by g-C<sub>3</sub>N<sub>4</sub>, charge density difference (CDD), adsorption energy of NO and effective charge of Bader were simulated based on DFT. Fig. 6(a) shows the g-C<sub>3</sub>N<sub>4</sub> and g-C<sub>3</sub>N<sub>4</sub>-Au models constructed for calculation. Fig. 6(b) shows the charge difference distribution of g-C<sub>3</sub>N<sub>4</sub> and g-C<sub>3</sub>N<sub>4</sub>-Au, with yellow areas indicating charge depletion and blue areas indicating charge accumulation. The change of charge in g-C<sub>3</sub>N<sub>4</sub> indicates that there is NO obvious electron transfer between the photocatalyst and NO, while there is obvious charge accumulation and charge consumption on g-C<sub>3</sub>N<sub>4</sub>-Au. The calculated Bader charge difference is used to study the charge conversion and electron redistribution between NO and photocatalysts. The accepted electron of NO increased from 0.19 e (g-C<sub>3</sub>N<sub>4</sub>) to 0.43 e (g-C<sub>3</sub>N<sub>4</sub>-Au), while the adsorption energy of NO molecule ( $E_{\text{ads}}$ ) decreased from -0.46 eV on g-C<sub>3</sub>N<sub>4</sub> to -2.31 eV on g-C<sub>3</sub>N<sub>4</sub>-Au. This indicates that NO, as an electron acceptor, is more likely to acquire electrons from g-C<sub>3</sub>N<sub>4</sub>-Au for adsorption and activation [13, 56]. The introduction of AuNPs not only reduces the band gap, but also facilitates the adsorption of NO, promotes electron transfer and thus promotes the photooxidation reaction. Fig. 6(c) and Fig. 6(d) show the calculated results of the main reaction pathways. We chose one main reaction:  $\text{NO} + \cdot\text{O}_2^- \rightarrow \text{NO}_3^-$ , and the Gibbs free energy of the lowest transition state ( $\Delta G_{\text{TS}}$ ) and Gibbs free energy of the reaction ( $\Delta G_{\text{rea}}$ ) in the photocatalytic reaction on g-C<sub>3</sub>N<sub>4</sub> and g-C<sub>3</sub>N<sub>4</sub>-Au were

calculated. Fig. 6(c) shows that the  $\Delta G_{TS}$  and  $\Delta G_{rea}$  in the reaction are 0.92 eV and -0.83 eV, respectively. The  $\Delta G_{TS}$  and  $\Delta G_{rea}$  of the reaction on g-C<sub>3</sub>N<sub>4</sub>-Au are 0.46 eV and -1.70 eV, indicating that the reaction requires a lower activation energy barrier and is more likely to occur. The negative  $\Delta G_{rea}$  indicates that the reaction can occur spontaneously, and the more negative the reaction is, the more likely it is to occur, and the energy release process exists in the reaction path. The calculation results proved that the reaction (7) on the photocatalyst surface was easier to carry out after the introduction of AuNPs, so more nitrate ions were generated and the photocatalytic activity of the catalyst was improved [41].

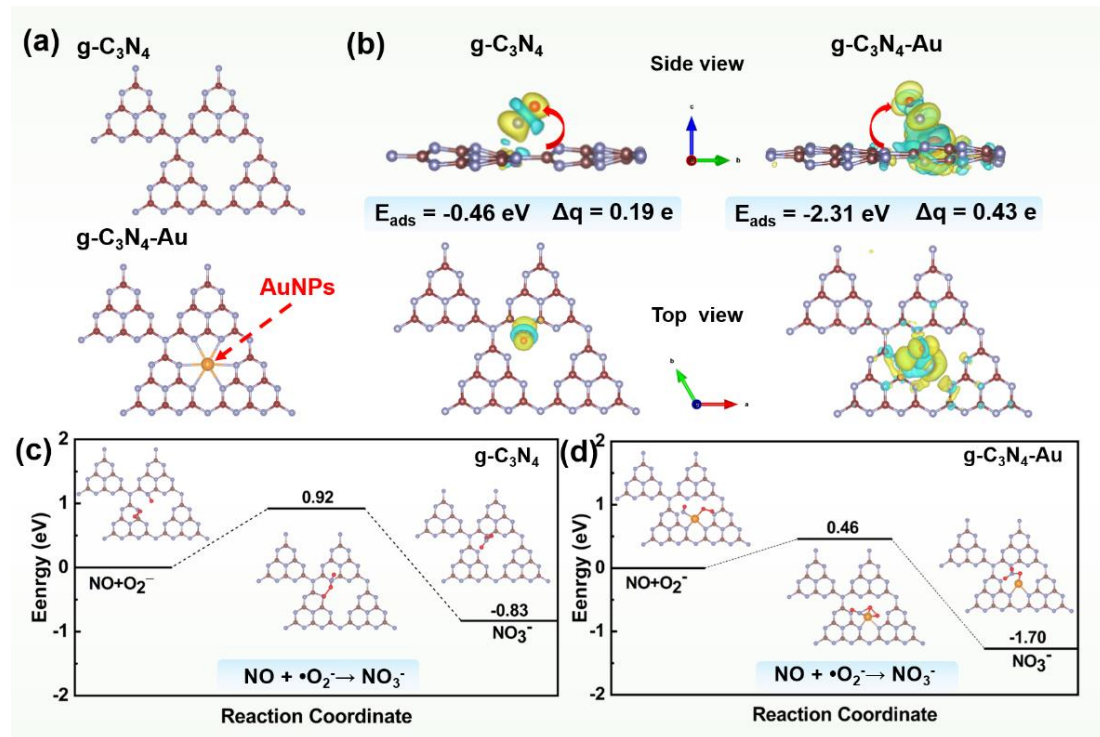


**Fig. 6** Analysis of the adsorption process of reactant molecules and reaction process: (a) the geometric structure of g-C<sub>3</sub>N<sub>4</sub> and g-C<sub>3</sub>N<sub>4</sub>-Au; red, blue, brown and yellow spheres represent O, N, C and Au atoms respectively; (b) the charge difference distribution when g-C<sub>3</sub>N<sub>4</sub> and g-C<sub>3</sub>N<sub>4</sub>-Au adsorb NO, where yellow represents charge depletion, blue indicates charge build-up.  $E_{ads}$  and  $\Delta q$  represent the calculated results of adsorption energy and Bader electron, respectively, (c, d) the calculated results of the main reaction pathways

#### 4. Conclusion

In this study, the g-C<sub>3</sub>N<sub>4</sub>-Au composite photocatalyst was successfully prepared

by photo-deposition method. Due to the SPR effect of Au nanoparticles, the visible light absorption capacity of the composites was significantly improved. By introducing Au nanoparticles to construct a heterojunction between Au nanoparticles and carbon nitride, a tight interface is formed between metal and semiconductor, promoting the SPR effect of Au, then enhanced the transfer of charge, improved the separation efficiency of electron-hole pairs, and prolonged the life of photogenerated carriers, so that the efficiency of NO oxidation removal was significantly improved. In addition, the main active species of catalytic oxidation process was confirmed by capture experiment as  $\bullet\text{O}_2^-$ . By optimizing the loading capacity of Au nanoparticles, under visible light irradiation, the oxidation removal ratio of NO remained 77.4 %, and the kinetic ratio constant was 4.32 times that of g-C<sub>3</sub>N<sub>4</sub>. In addition, g-C<sub>3</sub>N<sub>4</sub>-Au-3 composites still maintain high oxidation activity, indicating that it has excellent stability. after four cycles. In addition, *in-situ* infrared spectroscopy and DFT calculation were used to explore the oxidation pathway of NO. The results indicate that the introduction of Au nanoparticles reduced the activation energy of the oxidation reaction, made the reaction easier to proceed, and the intermediate products were reduced, and most of NO was eventually converted into nitrate, and accumulated on the surface of the composites.

#### **CRedit authorship contribution statement**

**Yanzhi Liu and Cheng Xie:** Writing - original draft, Methodology, Investigation.  
**Lei Xu:** Writing- Reviewing and Editing, Supervision, Funding acquisition. **Qianjun Ye:** Validation. **Bochuan Zhang:** Validation. **Mickael Capron and Vitaly Ordonsky:** Reviewing and Editing.

#### **Declaration of Competing Interest**

The authors declare that they have no known competing financial interests or personal relationships that could have appeared to influence the work reported in this paper.

#### **Acknowledgments**

This work was financially supported by the National Natural Science Foundation of China (Grant Nos. 51864030), and by National Key R&D Program of China (Nos. 2018YFC1901904), and by Yunnan Fundamental Research Projects (Nos. 202301AV070009 and Nos. 202101AS070023), and by Yunnan Provincial Science and Technology Talents Program (Nos. 2019HB003), and by Yunnan Provincial youth top-notch talent support program.

## References

- [1] Aminul Islam, Siow Hwa Teo, Chi Huey Ng, Yun Hin Taufiq-Yap, Shean Yaw Thomas Choong, Md. Rabiul Awual, Progress in recent sustainable materials for greenhouse gas (NO<sub>x</sub> and SO<sub>x</sub>) emission mitigation, *Progress in Materials Science* 32 (2023) 101033.
- [2] Jiahui Xian, Suisheng Li, Hui Su, Peisen Liao, Shihan Wang, Yawei Zhang, Wenqian Yang, Jun Yang, Yamei Sun, Yaling Jia, Qinglin Liu, Prof. Qinghua Liu, Prof. Guangqin Li, Electrocatalytic Synthesis of Essential Amino Acids from Nitric Oxide Using Atomically Dispersed Fe on N-doped Carbon , *Angewandte Chemie International Edition* 62 (2023) 1 of 9.
- [3] Xi Zhou, Jin Zhang, Xuemei Wang, Tianqi Tan, Ruimei Fang, Si Chen, Fan Dong, Efficient NO removal and photocatalysis mechanism over Bi-metal@Bi<sub>2</sub>O<sub>2</sub>[BO<sub>2</sub>(OH)] with oxygen vacancies, *Journal of Hazardous Materials* 436 (2022) 129271.
- [4] Minh-Thuan Pham, Adnan Hussain, Dai-Phat Bui, Truc-Mai Thi Nguyen, Sheng-Jie You, Ya-Fen Wang, Truc-Mai Thi Nguyen, Surface plasmon resonance enhanced photocatalysis of Ag nanoparticles-decorated Bi<sub>2</sub>S<sub>3</sub> nanorods for NO degradation, *Environmental Technology & Innovation*, 23 (2021) 101755.
- [5] Guangzhi He, Zhihua Lian, Yunbo Yu<sup>1</sup>, Yang Yang, Kuo Liu, Xiaoyan Shi, Zidi Yan, Wenpo Shan, Hong He, Polymeric vanadyl species determine the low-temperature activity of V-based catalysts for the SCR of NO<sub>x</sub> with NH<sub>3</sub>, *Science Advances* 4 (2018) 4637 .
- [6] Fadi Alakhras, Eman Alhajri, Redouane Haounati, Hassan Ouachtak, Abdelaziz Ait Addi, Tawfik A. Saleh, A comparative study of photocatalytic degradation

- of Rhodamine B using natural-based zeolite composites, *Surfaces and Interfaces* 20 (2020) 100611.
- [7] Bingnan Yuan, Yanan Wang, Ashraf Y. Elnaggar, Islam H. El Azab, Mina Huang, M. H. H. Mahmoud, Salah M. El-Bahy and Minghui Guo, Physical vapor deposition of graphitic carbon nitride (g-C<sub>3</sub>N<sub>4</sub>) films on biomass substrate: optoelectronic performance evaluation and life cycle assessment, *Advanced Composites and Hybrid Materials* 5 (2022) 813-822.
- [8] Jie Chen, Daming Zhao, Zhidan Diao, Miao Wang, Shaohua Shen, Ferrites boosting photocatalytic hydrogen evolution over graphitic carbon nitride: a case study of (Co, Ni) Fe<sub>2</sub>O<sub>4</sub> modification, *Science Bulletin* 61 (2016) 292-301.
- [9] Jing Tang, Rongping Xu, Guozhe Sui, Dongxuan Guo, Zhenlong Zhao, Shanshan Fu, Xue Yang, Yue Li, Jinlong Li, Double-Shelled Porous g-C<sub>3</sub>N<sub>4</sub> Nanotubes Modified with Amorphous Cu-Doped FeOOH Nanoclusters as 0D/3D Non-Homogeneous Photo-Fenton Catalysts for Effective Removal of Organic Dyes, *Small* 19 (2023) 2208232.
- [10] Guohui Dong, Liaoliao Zhao, Xiaoxia Wu, Mingshan Zhu, Fu Wang, Photocatalysis removing of NO based on modified carbon nitride: The effect of celestite mineral particles, *Applied Catalysis B: Environmental* 245 (2019) 459-468.
- [11] Yanglin Chen, Limo He, Hui-Ru Tan, Xuanhao Lin, Stephan Jaenicke and Gaik-Khuan Chuah, Molten salt synthesis of a highly crystalline graphitic carbon nitride homojunction from a deep eutectic solvent for selective photocatalytic oxidation, *Journal of Materials Chemistry A* 11 (2023) 12342-12353.
- [12] Trishamoni Kashyap, Sritam Biswas, Shahnaz Ahmed, Dhruvajyoti Kalita, Pabitra Nath, Biswajit Choudhury, Plasmon activation versus plasmon quenching on the overall photocatalytic performance of Ag/Au bimetal decorated g-C<sub>3</sub>N<sub>4</sub> nanosheets under selective photoexcitation: A mechanistic understanding with experiment and theory, *Applied Catalysis B: Environmental* 298 (2021) 120614.
- [13] Zheng Qi, Jinbao Chen, Weichuang Zhou, Yuhan Li, Xiaofang Li, Sushu Zhang,

- Jiajie Fan, Kangle Lv, Synergistic effects of holey nanosheet and sulfur-doping on the photocatalytic activity of carbon nitride towards NO removal, *Chemosphere* 316 (2023) 137813.
- [14] Xiao Zhang, Katarzyna Matras-Postolek, Heterojunction nanoarchitectonics of  $\text{WO}_x/\text{Au-g-C}_3\text{N}_4$  with efficient photogenerated carrier separation and transfer toward improved NO and benzene conversion, *Materials Today Advances* 17 (2023) 100355.
- [15] Peifang Wang, Xiang Guo, Lei Rao, Chao Wang, Yong Guo, Lixin Zhang, A weak-light-responsive  $\text{TiO}_2/\text{g-C}_3\text{N}_4$  composite film: photocatalytic activity under low-intensity light irradiation, *Environment Science Pollution Research* 25 (2018) 20206–20216.
- [16] Zhiying Guo, Fangxu Dai, Huixiang Yin, Mingming Zhang, Jun Xing, Lei Wang, The dual role of Au nanoparticles in the surface plasmon resonance enhanced photocatalyst  $\text{Au/g-C}_3\text{N}_4$ , *Colloid and Interface Science Communications* 48 (2022) 100615.
- [17] Yunqing Zhu, Tian Wang, Tao Xu, Yingxuan Li, Chuanyi Wang, Size effect of Pt co-catalyst on photocatalytic efficiency of  $\text{g-C}_3\text{N}_4$  for hydrogen evolution, *Applied Catalysis B Environmental* 464 (2019) 36-42.
- [18] Weiwen Wang, Delu Zhang, Pengxia Sun, Zhengnan Ji, Jihai Duan, High efficiency photocatalytic degradation of indoor formaldehyde by  $\text{Ag/g-C}_3\text{N}_4/\text{TiO}_2$  composite catalyst with ZSM-5 as the carrier, *Microporous and Mesoporous Materials* 322 (2021) 111134.
- [19] Kanglu Li, Wen Cui, Jieyuan Li, Yanjuan Sun, Yinghao Chu, Guangming Jiang, Ying Zhou, Yuxin Zhang, Fan Dong, Tuning the reaction pathway of photocatalytic NO oxidation process to control the secondary pollution on monodisperse Au nanoparticles@ $\text{g-C}_3\text{N}_4$ , *Chemical Engineering Journal* 378 (2019) 122184.
- [20] M. Faisal, Md A Rashed, Jahir Ahmed, Mabkhoot Alsaiari, Mohammed Jalalah S A Alsareii, Farid A Harraz, Au nanoparticles decorated polypyrrole-carbon black/ $\text{g-C}_3\text{N}_4$  nanocomposite as ultrafast and efficient visible light photocatalyst,

Chemosphere 287 (2022) 131984.

- [21] G.Kresse, J. Furthmüller, Efficiency of ab-initio total energy calculations for metals and semiconductors using a plane-wave basis set, *Computational Materials Science* 1 (1996) 15-50.
- [22] G.Kresse, J. Furthmüller, Efficient iterative schemes for ab initio total-energy calculations using a plane-wave basis set, *Physical Review B* 16 (1996) 11169-11186.
- [23] Perdew, Burke, Ernzerhof, Generalized gradient approximation made simple. *Physical Review Letters* 18 (1996) 3865-3868
- [24] Hendrik J. Monkhorst and James D. Pack , Special Points for Brillouin-Zone Integrations. *Physical Review B* 13 (1976) 5188-5192.
- [25] P E Blochl, Projector Augmented-Wave Method, *Physical Review B* 50 (1994) 17953-17979.
- [26] Stefan Grimme , Jens Antony , Stephan Ehrlich , Helge Krieg , A Consistent and Accurate ab Initio Parametrization of Density Functional Dispersion Correction (DFT-D) for the 94 Elements H-Pu, *Journal of Chemical Physics* 132 (2010) 154104.
- [27] Linlin Xu, Qingqiang Cui, Yue Tian, Anxin Jiao, Mengya Zhang, Shuang Li, Hengshuai Li, Ming Chen, Enhanced synergistic coupling effect of ternary Au/Ag/AgCl nanochains for promoting natural-solar-driven photocatalysis, *Applied Surface Science* 545 (2021) 149054.
- [28] Xin Li, Haopeng Jiang, Changchang Ma, Zhi Zhu, Xianghai Song, Huiqin Wang, Pengwei Huo, Xiuyan Li, Local surface plasma resonance effect enhanced Z-scheme ZnO/Au/g-C<sub>3</sub>N<sub>4</sub> film photocatalyst for reduction of CO<sub>2</sub> to CO, *Applied Catalysis B: Environmental* 283 (2021) 119638.
- [29] Zhou Chen, Xiang Yu, Qiuhui Zhu, Tingting Fan, Qiuling Wu, Lizhong Zhang, Jianhui Li, Weiping Fang, Xiaodong Yi, Steam engraving optimization of graphitic carbon nitride with enhanced photocatalytic hydrogen evolution, *Carbon* 139 (2018) 189-194.
- [30] He Zhao, Xiaoling Ding, Bing Zhang, Yingxuan Li, Chuanyi Wang, Enhanced

- photocatalytic hydrogen evolution along with byproducts suppressing over Z-scheme  $Cd_xZn_{1-x}S/Au/g-C_3N_4$  photocatalysts under visible light, *Science Bulletin* 62 (2017) 602-609.
- [31] Yanzhao Zou, Yang Xie, Shan Yu, Lvcun Chen, Wen Cui, Fan Dong, Ying Zhou,  $SnO_2$  quantum dots anchored on  $g-C_3N_4$  for enhanced visible-light photocatalytic removal of NO and toxic  $NO_2$  inhibition, *Applied Surface Science* 496 (2019) 143630.
- [32] Wei Zhao, Qian Dong, Cheng Sun, Dehua Xia, Haibao Huang, Gang Yang, Guoxiang Wang, Dennis Y.C.Leung, A novel  $Au/g-C_3N_4$  nanosheets/ $CeO_2$  hollow nanospheres plasmonic heterojunction photocatalysts for the photocatalytic reduction of hexavalent chromium and oxidation of oxytetracycline hydrochloride, *Chemical Engineering Journal* 409 (2021) 128185.
- [33] Meng Shen, Lingxia Zhang, Min Wang, Jianjian Tian, Xixiong Jin, Limin Guo, Lianzhou Wang and Jianlin Shi, Carbon-vacancy modified graphitic carbon nitride: enhanced  $CO_2$  photocatalytic reduction performance and mechanism probing, *Journal of Materials Chemistry A* 7 (2019) 1556-1563.
- [34] Yazhou Zhang, Zhenxiong Huang, Chung-Li Dong, Jinwen Shi, Cheng Cheng, Xiangjiu Guan, Shichao Zong, Bing Luo, Zening Cheng, Daixing Wei, Yu-cheng Huang, Shaohua Shen, Liejin Guo, Synergistic effect of nitrogen vacancy on ultrathin graphitic carbon nitride porous nanosheets for highly efficient photocatalytic  $H_2$  evolution, *Chemical Engineering Journal* 431 (2022) 134101.
- [35] Benlin Dai, Xin Chen, Xiaofan Yang, Gang Yang, Shijie Li, Lili Zhang, Feihu Mu, Wei Zhao, Dennis Y.C. Leung, Designing S-scheme  $Au/g-C_3N_4/BiO_{1.2}I_{0.6}$  plasmonic heterojunction for efficient visible-light photocatalysis, *Separation and Purification Technology* 287 (2022) 120531.
- [36] Shujuan Jiang, Chuanbao Xiong, Shaoqing Song, and Bei Cheng, Plasmonic Graphene-Like  $Au/C_3N_4$  Nanosheets with Barrier-Free Interface for Photocatalytically Sustainable Evolution of Active Oxygen Species, *ACS Sustainable Chemistry & Engineering* 7 (2019) 2018-2026.

- [37] Guangming Jiang, Xinwei Li, Mengna Lan, Ting Shen, Xiaoshu Lv, Fan Dong, Sen Zhang, Monodisperse bismuth nanoparticles decorated graphitic carbon nitride: Enhanced visible-light-response photocatalytic NO removal and reaction pathway, *Applied Catalysis B: Environmental* 205 (2017) 532–540.
- [38] Arteaga-Pérez L E, Manrique R, Castillo-Puchi F, Ortega M, Bertiola C, Pérez A, Jiménez R, One-pot amination of cyclohexanone-to-secondary amines over carbon-supported pb: Unraveling the reaction mechanism and kinetics, *Chemical Engineering Journal* 417 (2021) 129236.
- [39] Yuhan Li, Yanjuan Sun, Wingkei Ho, Yuxin Zhang, Hongwei Huang, Qiang Cai, Fan Dong. Highly enhanced visible-light photocatalytic NO<sub>x</sub> purification and conversion pathway on self-structurally modified g-C<sub>3</sub>N<sub>4</sub> nanosheets, *Science Bulletin* 63 (2018) 609-620.
- [40] Guimei Liu, Ying Huang, Haiqin Lv, Hui Wang, Yubin Zeng, Mingzhe Yuan, Qingguo Meng, Chuanyi Wang. Confining single-atom Pd on g-C<sub>3</sub>N<sub>4</sub> with carbon vacancies towards enhanced photocatalytic NO conversion, *Applied Catalysis B: Environmental* 284 (2021) 119683.
- [41] Lizhen Hu, Teng Wang, Qianqian Nie, Jiayou Liu, Yunpei Cui, Kefei Zhang, Zhongchao Tan, Hesheng Yu, Single Pd atoms anchored graphitic carbon nitride for highly selective and stable photocatalysis of nitric oxide, *Carbon* 200 (2022) 187-198.
- [42] Zhihuan Zhao, Jimin Fan, Wenhui Liu, Yongqiang Xue, Shu Yin, *In-situ* hydrothermal synthesis of Ag<sub>3</sub>PO<sub>4</sub>/g-C<sub>3</sub>N<sub>4</sub> composite and their photocatalytic decomposition of NO<sub>x</sub>, *Journal of Alloys and Compounds* 695 (2017) 2812-2819.
- [43] Jundie Hu, Yujin Ji, Zhao Mo, Najun Li, Qingfeng Xu, Youyong Li, Hui Xu, Dongyun Chen, Jianmei Lu, Engineering black phosphorus to porous g-C<sub>3</sub>N<sub>4</sub>-metal-organic framework membrane: a platform for highly boosting photocatalytic performance, *Journal of Materials Chemistry A* 7 (2019) 4408–4414.
- [44] Wen Cui, Wenjia Yang, Peng Chen, Lvcun Chen, Jieyuan Li, Yanjuan Sun,

- Ying Zhou, Fan Dong, Earth-abundant  $\text{CaCO}_3$ -based photocatalyst for enhanced ROS production, toxic by-product suppression, and efficient NO removal, *Energy & Environmental Materials* 5 (2022) 928–934.
- [45] Guping Zhang, Xingwang Zhu, Dongyun Chen, Najun Li, Qingfeng Xu, Hua Li, Jinghui He, Hui Xu, Jianmei Lu, Hierarchical Z-scheme  $\text{g-C}_3\text{N}_4/\text{Au}/\text{ZnIn}_2\text{S}_4$  photo-catalyst for highly enhanced visible-light photocatalytic nitric oxide removal and carbon dioxide conversion, *Environmental Science-Nano* 2 (2022) 676–687.
- [46] Tong Wang, Wenhan Yang, Lu Chang, Hao Wang, Huan Wu, Jinrong Cao, Hua Fan, Jingquan Wang, Haitao Liu, Yunhu Hou, Ru Zhang, Zhimao Yang, Hao Zhu, Chuncai Kong, One-step calcination synthesis of accordion-like MXene-derived  $\text{TiO}_2@\text{C}$  coupled with  $\text{g-C}_3\text{N}_4$ : Z-scheme heterojunction for enhanced photocatalytic NO removal, *Separation and Purification Technology* 285 (2022) 120329.
- [47] Xiang Xia, Baogang Xu, Hongyu Zhang, Kang Ji, Xingshuai Ji, Dan Wang, Ping Yang,  $\text{NiCoP}/\text{g-C}_3\text{N}_4$  Schottky heterojunctions towards efficient photocatalytic NO oxidation, *Journal of Alloys and Compounds* 928 (2022) 167207.
- [48] Dongni Liu, Dongyun Chen, Najun Li, Qingfeng Xu, Hua Li, Jinghui He, Jianmei Lu, Integration of 3D macroscopic graphene aerogel with 0D-2D  $\text{AgVO}_3@\text{g-C}_3\text{N}_4$  heterojunction for highly efficient photocatalytic oxidation of nitric oxide, *Applied Catalysis B: Environmental*, 243 (2019) 576–584.
- [49] Chinh Van Tran, Duong Duc La, Phuong Nguyen Thi Hoai, Ha Duc Ninh, Phuong Nguyen Thi Hong, Thu Ha T Vu, Ashok Kumar Nadda, X Cuong Nguyen, D Duc Nguyen, Huu Hao Ngo, New  $\text{TiO}_2$ -doped Cu–Mg spinel-ferrite-based photocatalyst for degrading highly toxic rhodamine B dye in wastewater, *Journal of Hazardous Materials* 420 (2021) 126636.
- [50] Mengtian Huang, Cong Chen, Ting Wang, Qi Sui, Kun Zhang, Benxia Li, Cadmium-sulfide/gold/graphitic-carbon-nitride sandwich heterojunction photocatalyst with regulated electron transfer for boosting carbon-dioxide

- reduction to hydrocarbon, *Journal of Colloid and Interface Science* 613 (2022) 575-586.
- [51] Peng Wen, Yinghui Sun, Hui Li, Zhiqiang Liang, Haihua Wu, Junchang Zhang, Huajie Zeng, Scott M Geyer, Lin Jiang, A highly active three-dimensional Z-scheme ZnO/Au/g-C<sub>3</sub>N<sub>4</sub> photocathode for efficient photoelectrochemical water splitting, *Nanoscale* 263 (2020) 118180.
- [52] Xin Yu, Xin Jin, Xuanyu Chen, Aizhu Wang, Jianming Zhang, Jian Zhang, Zhenhuan Zhao, Mingming Gao, Luca Razzari and Hong Liu, A Microorganism Bred TiO<sub>2</sub>/Au/TiO<sub>2</sub> Heterostructure for Whispering Gallery Mode Resonance Assisted Plasmonic Photocatalysis, *ACS Nano* 14 (2020) 13876-13885.
- [53] Wei Zhao, Sisi Ma, Gang Yang, Guoxiang Wang, Lili Zhang, Dehua Xia, Haibao Huang, Zhipeng Cheng, Jiming Xu, Cheng Sun, Dennis Y.C. Leung, Z-scheme Au decorated carbon nitride/cobalt tetroxide plasmonic heterojunction photocatalyst for catalytic reduction of hexavalent chromium and oxidation of Bisphenol A, *Journal of Hazardous Materials* 410 (2021) 124539.
- [54] Yanyan Shang, Huiqing Fan, Xiuzi Che, Weijia Wang, Promoted photocatalytic hydrogen evolution via double-electron migration in Ag@g-C<sub>3</sub>N<sub>4</sub> heterojunction, *International Journal of Hydrogen Energy* 48 (2023) 17370-17382.
- [55] Jifang Cui, Xuebin Lu, Mengyan Guo, Ming Zhang, Linhao Sun, Jian Xiong, Rui Zhang, Xiaoyun Li, Yina Qiao, Dan Li, Mingyu Guo, Zhihao Yu, Construction of a g-C<sub>3</sub>N<sub>4</sub>-driven photocatalytic system for boosted biomass-derived alcohol oxidation: a promising route towards sustainable biomass valorization, *Catalysis Science & Technology* 13 (2023) 940.
- [56] Maoxi Ran, Peng Chen, Jiarui Li, Wen Cui, Jieyuan Li, Ye He, Jianping Sheng, Yanjuan Sun, Fan Dong, Promoted reactants activation and charge separation leading to efficient photocatalytic activity on phosphate/potassium co-functionalized carbon nitride, *Chinese Chemical Letters* 30 (2019) 875-880.
- [57] Jiarui Li, Wendong Zhang, Maoxi Ran, Yanjuan Sun, Hongwei Huang, Fan Dong, Synergistic integration of Bi metal and phosphate defects on hexagonal and monoclinic BiPO<sub>4</sub>: Enhanced photocatalysis and reaction mechanism,

- Applied Catalysis B: Environmental 243 (2019) 313-321.
- [58] Jeffrey C.S. Wu, Yu-Ting Cheng, *In-situ* FTIR study of photocatalytic NO reaction on photocatalysts under UV irradiation, Journal of Catalysis 237 (2006) 393–404.
- [59] Huizhong Wu, Chaowei Yuan, Ruimin Chen, Jiadong Wang, Fan Dong, Jieyuan Li, and Yanjuan Sun, Mechanisms of Interfacial Charge Transfer and Photocatalytic NO Oxidation on BiOBr/SnO<sub>2</sub> p–n Heterojunctions, ACS Applied Materials & Interfaces 12 (2020) 43741–43749.